# PROCEEDINGS OF SPIE

SPIEDigitalLibrary.org/conference-proceedings-of-spie

# High-speed in-line optical angular scatterometer for high-throughput roll-to-roll nanofabrication

Faria-Briceno, Juan, Sasidharan, Vineeth, Neumann, Alexander, Singhal, Shrawan, Sreenivasan, S. V., et al.

Juan J. Faria-Briceno, Vineeth Sasidharan, Alexander Neumann, Shrawan Singhal, S. V. Sreenivasan, S. R. J. Brueck, "High-speed in-line optical angular scatterometer for high-throughput roll-to-roll nanofabrication," Proc. SPIE 11610, Novel Patterning Technologies 2021, 116100F (22 February 2021); doi: 10.1117/12.2593730



Event: SPIE Advanced Lithography, 2021, Online Only

## High-Speed In-line Optical Angular Scatterometer for High-Throughput Roll-to-Roll Nanofabrication

Juan J. Faria-Briceno<sup>a</sup>, Vineeth Sasidharan<sup>a</sup>, Alexander Neumann<sup>a</sup>, Shrawan Singhal<sup>b</sup>, S.V. Sreenivasan<sup>b</sup> and S. R. J. Brueck<sup>a</sup>

<sup>a</sup> Center for high Technology and Materials and Department of Electrical and Computer Engineering, University of New Mexico, Albuquerque, 1313 Goddard St. SE, Albuquerque, New Mexico 87106, USA. <sup>b</sup>NASCENT ERC and Department of Mechanical Engineering, University of Texas at Austin, 10100 Burnet Rd, Austin, TX 78758. Correspondence and requests for materials should be sent to J.J.F.B. (email: jfaria@unm.edu)

#### **ABSTRACT**

Roll-to-roll and other high-speed printing manufacturing processes are increasingly being extended to micro- and nanoelectronics and photonics due to cost and throughput advantages as compared with traditional wafer-scale manufacturing. The extra degrees of freedom associated with a moving web require high speed, in-line metrology to control the manufacturing process. Many state-of-the-art metrology approaches have sub-10 nm resolution but cannot be implemented during real-time fabrication processes because of environmental constraints or contact/cross sectional requirements. Optical angular scatterometry is a non-contact metrology approach that can be implemented at high speed. We demonstrate a system that uses  $45^{\circ}$  off-axis parabolic mirrors and an 8kHz resonant scanner to vary the incident/reflected angle from  $\sim 17^{\circ}$  to  $\sim 67^{\circ}$ , suitable for nanoscale metrology at web speeds of up to 350 cm/s, well-beyond the speed of current manufacturing tools. Scatterometry is sensitive not only to gross defects (missing pattern sections) but also to variations in nanoscale pattern details, offering a pathway to feedback control of the manufacturing process.

#### 1. INTRODUCTION

Wafer-scale integrated circuit manufacturing has progressed to single-digit nanometer scales with increasing complex topologies including FINFETs and gate-all-around (GAA) transistors requiring new approaches to metrology. Largearea, high-throughput, low-cost alternative techniques such as roll-to-roll (R2R) and other printed electronics approaches are being extended to the fabrication (sub-50 nm) of wire-grid polarizers, metal-mesh grids, metamaterials, battery storage, and other devices <sup>4-6</sup>. In contrast to wafer-scale manufacturing where a robust tool set and a stable wafer platform often enable statistical process control strategies <sup>1</sup>, the extra degrees of freedom associated with a flexible web demand real-time, on-line metrology strategies. <sup>4</sup>

Off-line ellipsometric,  $^{7-8}$  and off-line angular systems are available for wafer-scale manufacturing. For R2R fabrication systems, at-line spectroscopic tools have been demonstrated showing the ability to characterize pattern structures in the fabrication module  $^{10}$ . However, this system required stopping the web to take large-area images, limiting its real-time, high—speed capabilities. A throughput limitation for spectroscopic and ellipsometric metrology tools is the requirement for wavelength scanning  $^{154}$ , which demands a relatively weak broadband source and typically mechanical (grating) wavelength scanning. Off-line angular scatterometry uses fixed wavelength laser source, but it requires sample stage movement; limiting its applicability to a moving web  $^9$ . Angular optical scatterometry is a noncontact technique with demonstrated sensitivity to  $\sim 10$ -nm scales that can be implemented on-line without disruption of the manufacturing process.  $^{11-14}$ 

In-line angular scatterometry has been demonstrated for real-time characterization; offering an angular range ~30° and using 90° off-axis parabolic mirrors to provide the angular sweep. <sup>15</sup> However, this system required mirrors located close to the moving web, increasing the chances of web fabrication interference. Yet more development was required to achieve proper data acquisition without fabrication interference with the moving web at large angular ranges (45° off-axis parabolic mirrors). Similar work has demonstrated real-time characterization of nano-scale structures using a CCD camera at 1 mm/s scanning speed (slow compared with our ~50 cm/s scanning capabilities) <sup>16</sup>.

In this paper, we demonstrate a high-speed, non-contact, non-destructive angular scatterometer for real-time characterization (for plane surfaces, 1D patterned and complex 2D patterned structures). Our system sweeps the angular incidence of a 405 nm laser beam using 45° off-axis parabolic mirrors. The angular range of the system is  $\sim 50^{\circ}$  with an initial angle of  $\sim 17^{\circ}$  and a final angle of 67° (this angular range can be adjusted by modifications of the optics). A higher angular range can be achieved by variation of the parabolic mirror positions (up to 80°). Our current arrangement, with 8.0 kHz resonant angular scanners obtains a reflectance spectrum every 62.5 ms. With an  $\sim 200$  Dm diameter spot size on the web, this is compatible with a web speed of up to 320 cm/s before the web has moved by a spot diameter. We designed for an anticipated web speed of  $\sim 50$  cm/s which allows averaging of up to 7 reflectance waveforms before the web has moved by a spot diameter. We demonstrate the capability of this angular optical scatterometer at a web speed of  $\sim 50$  cm/s using a reciprocating stage.

#### 2. EXPERIMENTAL SET UP

#### 2.1 Overview Optical Design

This in-line optical angular scatterometer provides real-time metrology without interfering with the fabrication process. The scan speed is compatible and faster ( $\sim 50$  cm/s) than currently projected fabrication speed of 10 cm/s. We collect the 0<sup>th</sup> order reflection from flat thin layers and periodic (1D and 2D structures) as a function of incident angle by focusing a polarized laser beam at the moving web. Fig. 1 presents the overall design of the in-line angular scatterometer using 45° off-axis parabolic mirrors. We use a 4.5 mW output power, collimated, single-transverse-mode diode laser with an elliptical beam profile of  $1.8\times3.5$  mm² and a spectral bandwidth of  $\sim 2.8$  nm. The laser beam can be polarized either TE or TM with respect to the plane of incidence onto the web. After the polarizer, a 40-cm focal length lens focuses the beam from the laser to the center of the resonant scanner mirror. The scanner oscillates at 8.0 kHz and has an angular span of  $\sim 20^\circ$ . A second, 100-mm diameter 30-cm focal length lens collimates the beam from the resonant scanner and directs it to a highNA 45° off-axis parabolic mirror.

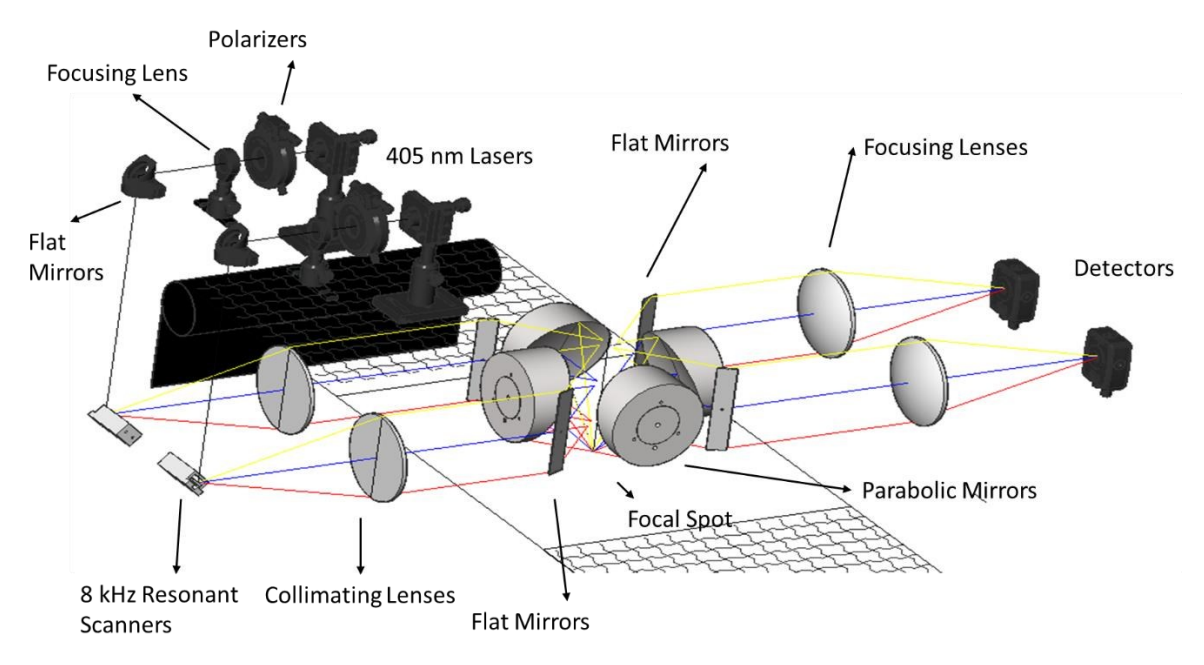


Fig. 1: In-line Angular scatterometer using 45° off-axis parabolic mirrors – overall optical design. Two lines scanning directions are required for fast line and width line. The yellow, blue and red beams are generated sequentially due to the rotation of the resonant scanner. The yellow beam is the smallest angle obtain from the system and the red is the largest angle obtained from the system. Figs. 1 and 2 show only the optical components related to beam path.

The parabolic mirror focuses the incident beam into the moving web with a total angular range of ~50° from  $\theta_i$  =~17° to  $\theta_f$ =~67°. The large-area parabolas are 101.6 mm in diameter with a focal length of 119.0 mm. At the center of the scan, the focal spot at the moving web is ~125×120 µm² and varies from ~85×70 µm² at 17° to ~200×190 µm² at 67° The reflected beam from the web is directed to a mirror image of the optical path and is focused onto a silicon PIN photodetector to collect the reflectivity as a function of angle.

The commercial 13 mm² area blue enhanced silicon PIN detector (Advance Photonix SD 290-12-22-241) is sensitive at the 405 nm wavelength and is reversed biased at 12 V to allow detection at 8 kHz. The signal is collected using an oscilloscope; the oscilloscope trace is digitized and transferred to a computer for analysis. The high-speed detection shown in Fig. 3 corresponds to  $\sim$  2 cycles of the mirror oscillation; each cycle corresponds to a sweep from low to high angles of incidence and the return. The number of resolvable angular points, the ratio of the beam NA to the overall system NA, is  $\sim$ 330 giving an angular resolution of  $\sim$ 0.14°.

#### 2.2 High-speed Actuator, High-Speed Data Collection, and Calibration

In order to simulate the high-speed fabrication web, we used both 5- and 100- RPM reciprocating actuators with a stroke of 2.5 cm to drive a linear stage. The peak velocity at the center of the stroke was  $\sim 2.5$ - and 50-cm/s. The reflectivity signal is obtained at the highest speed of the stage using a reference signal generated from a trigger synced to the actuator motion. Fig. 2 shows the high-speed ray tracing of the scope and the reference signal used to find the max speed. The full push/pull of the fast (slow) actuator creates a periodic signal with a 600 ms (12 sec) period. At 300 ms, the reflection as a function of angle is extracted to prove the scanning capabilities of our system at a speed of 50 cm/s. At  $\sim$ 50 (2.5) cm/s, 7 (140) waveforms were averaged to reduce noise on the final experimental signal.

Due to all the optical components associated with the system, the in-line tool requires calibration. To establish the calibration, we compare the reflectivity of a well-defined flat surface sample measured on both the in-line and the off-line scatterometry systems (similar to the process reported previously). <sup>15</sup> A silicon substrate was cleaned using HF and Piranha to remove all contamination (native oxide and organic contamination). Then 4.9 nm thick alumina (Al<sub>2</sub>O<sub>3</sub>) layer was deposited onto the silicon wafer. The thickness of the alumina layer was characterized using ellipsometry. The calibration was derived from:

$$C(\theta) = I - Iof fin((\theta\theta)) \times RRoffin((\theta\theta))$$
 (1)



Fig. 2: Scope ray tracing showing high-speed detection of reflection from sample as function of angle, and reference signal from second laser source to find top speed of the actuator movement. a) Zoom of the reflection as function of angle when the sample stage position blocks the laser beam reference signal. b) Experimental image of the actuator, laser beam, and sample stage.  $I_{off}$  is the incident beam intensity for the off-line scatterometer system before the sample.  $R_{off}$  is the reflected beam intensity for the off-line scatterometer system.  $I_{in}$  is the incident beam intensity for in-line scatterometer system.  $R_{in}$  is the reflected beam intensity for in-line scatterometer system from the sample.  $C(\theta)$  is the calibration curve. Fig. 3 presents the calibration coefficient vs. incident angle for TE and TM polarization. The local variation around 37° is related to contamination on the optics. All experimental data is normalized to the instantaneous laser power, monitored with a separate photodetector, and then multiplied by the appropriate TE or TM calibration curve.

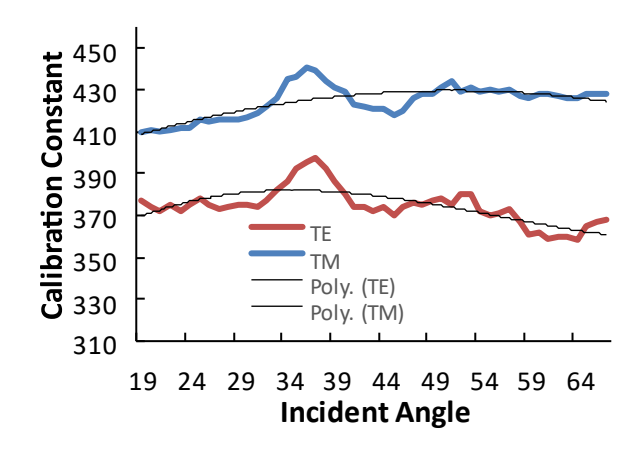
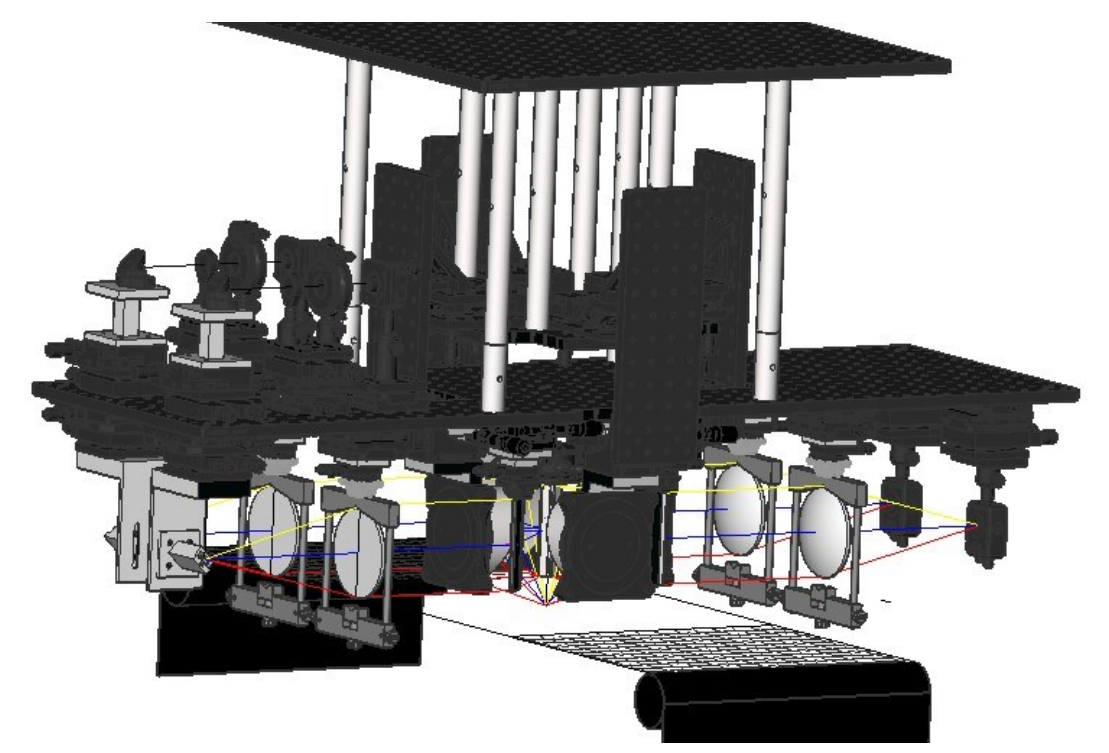


Fig. 3: Calibration coefficient vs. incident angle for TE and TM polarization obtain from the system using a well-known thin Alumina layer sample.

#### 2.3 Overview Full Design with Mount and Stages and System Configurations

Each optical component was adjustable in at least five or six axes to allow alignment. Tip, tilt, rotation and translation stages were added to control each component individually. The mechanical system was suspended on top of the moving stage allowing measurement of the reflectivity curve as a function of angle without interfering with the fabrication process. The length, width and height of the system are  $\sim 1$ -, 0.4-, and 0.9- m, respectively with a total volume of  $\sim 0.36$  m<sup>3</sup>. Fig. 4 presents the full design of the in-line scatterometer with all components suspended in the air. Fig. 5 shows the full experimental set up. The angular range can be increased by reducing the 45° off-axis parabolic mirror focal length. However, the shorter the focal length, the closer the proximity to the web complicating the arrangement of the optical parts and requiring a revised design of the system.

There are several options for data acquisition relative to the web speed. The most demanding in terms of speed is taking the data before the web moves by a spot size, which allows averaging of up to 30 waveforms at the 10 cm/s design speed, and 6 waveforms at the 50 cm/s demonstrated speed. We are presently only averaging in the forward scan  $(17^{\circ} \text{ to } 67^{\circ})$  and have not addressed issues of lag in the reverse direction. Alternatively, the average can be extended to  $\sim 8000$  (1 sec) to be commensurate with data transfer and analysis time, providing a running measurement to monitor for drift of the manufacturing process. The system can detect both gross defects (e.g. missing/malformed patterns) and subtle pattern details (e.g. linewidth variations) that often indicate drift of the manufacturing process and can be used for real-time feedback control.



Proc. of SPIE Vol. 11610 116100F-4

Fig. 4: Full design with all rotation, translation, tilt, tip stages with custom made mounts on top of R2R web stage.

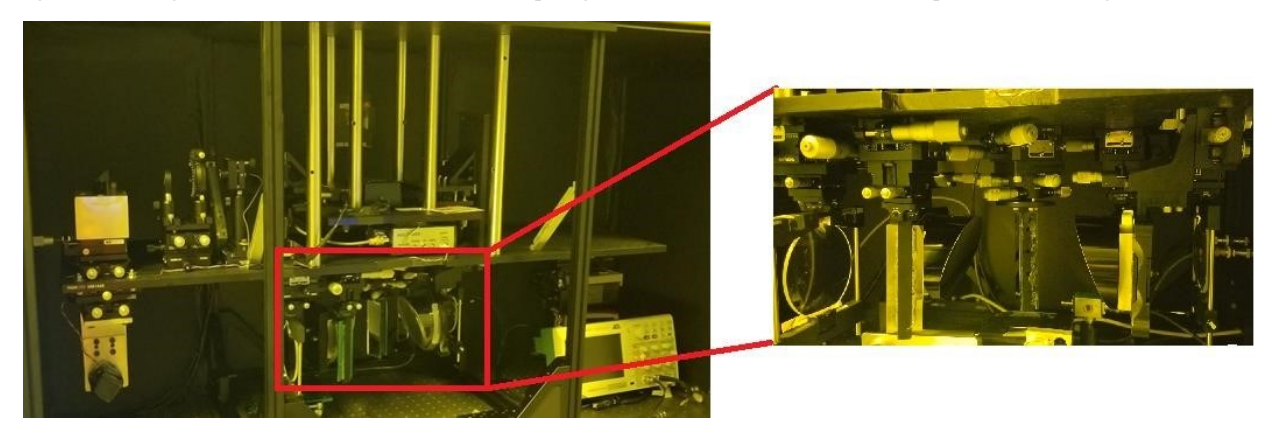


Fig. 5: Experimental in-line angular scatterometer setup (zoom of the center area including: parabolic mirrors, flat mirrors, collimating lenses, custom stages, and commercial multi-stages).

#### 3. SAMPLES

Four different samples were used to demonstrate real-time operation of the in-line scatterometer. The samples are silicon wafers with thin films of native and thermal oxide, 1-dimensional undercut Al lines (1D), and 2-dimensional (2D) complex silicon nanotubes. All samples were compared between the off-line and the in-line scatterometer. Although R2R nanopatterning processes normally are carry out on flexible polymer which provide anisotropic optical conditions and lower reflectance than silicon wafer, our samples are on silicon substrates for practical purposes. We have previously demonstrated on our off-line angular scatterometer the scanning capabilities of low reflectance substrates (polycarbonate)

<sup>9</sup>. The samples were fabricated by using thermal oxidation, interferometric lithography (IL), and Nano-imprint lithography (NIL) (details in Methods section below). Thin films were fabricated and characterized using ellipsometry. A thin film calculation was used to compare with our experimental off-line, and in-line results. RCWA was used to fit the 1D structures; only experimental results are shown for the complex 2D structures. The experimental results and the simulation were compared by calculating the lowest Root Mean Square Error (RMSE). All patterned structures were compared by using SEM characterization, off-line angular scatterometry, and in-line 8.0 kHz scatterometer. Fig. 6 presents the side view SEM image of the 1D undercut Al lines. Fig. 7 presents the 2D complex silicon nanotubes a) SEM side view, b) 4" wafer top view, c) side-view structural diagram, and d) top-view structural diagram.

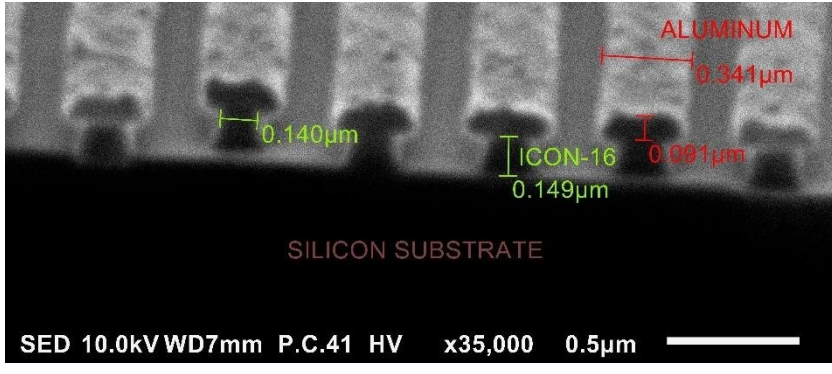


Fig. 6: Side View of the undercut 1D Al lines 15.

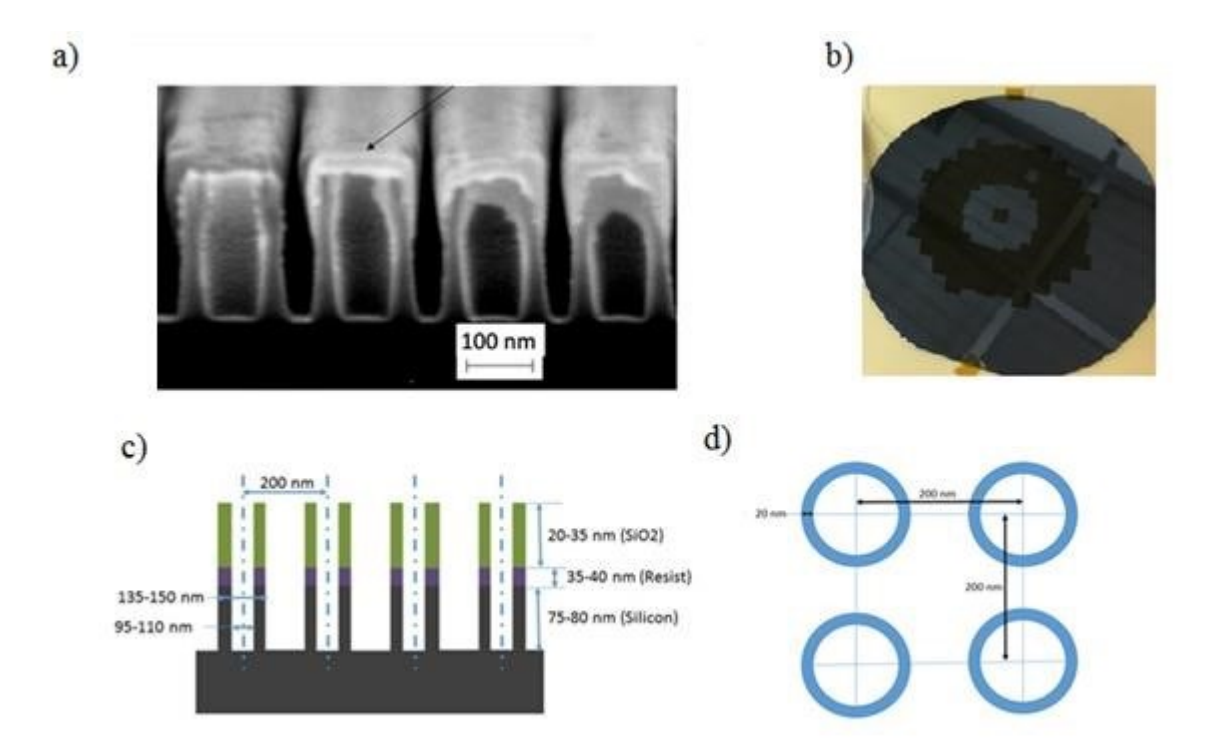


Fig. 7: 2D complex silicon nanotubes fabricated using NIL: a) side-view SEM image, b) 4" wafer top view, c) side-view structure diagram (the film on top of the cylinders is due to the gold flash coating for the SEM and is not present for the scatterometry measurements), and d) top-view structural diagram <sup>15</sup>.

#### 4. FABRICATION

#### 4.1 Thin Layer Samples

One thin layer sample is a silicon substrate with a thin layer of native oxide. The second thin layer sample is a commercially available (J.A. Woollam) silicon wafer with  $\sim 115$  nm thermally grown  $SiO_2$  layer. Both were characterized using ellipsometry and compared to our experimental results fitting using a thin layer calculation and fitted to the experimental results. Native and thermally grown oxide optical properties were used accordingly for proper simulation  $^{17}$ .

#### 4.2 1D Undercut Al Lines

Interferometric Lithography (IL) was used for the 1D samples. IL is low cost, large area capability, short exposure time, simplicity, and flexibility.  $^{18}$  The substrate is Si and it was cleaned by using acetone, methanol, and isopropyl. A layer of antireflective coating (BARC); the BARC ICON 16 layer was spin at 3000 rpm for 30 seconds and baked at 190 °C for 60 seconds (thickness of ~160 nm). Negative photoresist (NR7-500) was spin at 3000 rpm for 30 seconds with a soft bake of 150 °C for 60 seconds (~500 nm thick). The sample was exposed to 355-nm frequency tripled YAG coherent laser for 8 seconds with a pattern period of ~500 nm. The total exposure dose was ~115 mJ/cm³ and developed with MF321 developer for a total time of 20 seconds. The sample was metalized by evaporating aluminum on the surface at a chamber pressure of 2×10-6 Torr (a ~85 nm) and followed by a lift-off process. BARC ICON 16 layer was etched with O2 plasma reactive ion etching (RIE) under a time of 90 seconds. The roughing pressure, RF power level, plasma power, and gas flow rate at 15 mT, 100 W, 300 W, and 21 sccm.

#### 4.3 2D Silicon Nanotubes:

The 2D silicon nanotubes were fabricated using NIL, atomic layer deposition (ALD), and reactive -ion etching (RIE). First step was to nanoimprint the photoresist pillars on the silicon wafer. Then, an  $SiO_2ALD$  was used to form the walls. The  $SiO_2$  acted as a mask while the silicon was etch away forming the nanotubes. Finally, RIE was implemented to remove the cap and the  $SiO_2$  that served as a mask while the silicon was removed to form the nanotubes.

#### 5. RESULTS AND DISCUSSION

All samples were measured under moving web conditions. The stage speed was set at ~50 cm/second. The experimental data was averaged over 6 forward scan waveforms to reduce noise. The repeatability of the measurements was proven by obtaining the experimental signal multiple times (3) at ~50 cm/s using the reference signal (laser beam reference signal). The output average waveform was normalized and calibrated to fit with the models. All results were fit to the lowest rootmean-square error (RMSE) to find best fit conditions.

#### 5.1 Silicon Wafer with Native Oxide

The thickness of the native oxide on the silicon wafer was measured by using ellipsometry and compared with off-line, and in-line scatterometers. The experimental curves were fitted to a thin layer model. The root-mean-square error (RMSE) was calculated to find the best fit. Fig. 8 present the a) TE and the b) TM reflection curve of 8.0 kHz in-line scatterometer (at 0, ~50 cm/second and off-line systems). Tables 1 and 2 present the RMSE from each system and the native oxide thickness obtained.

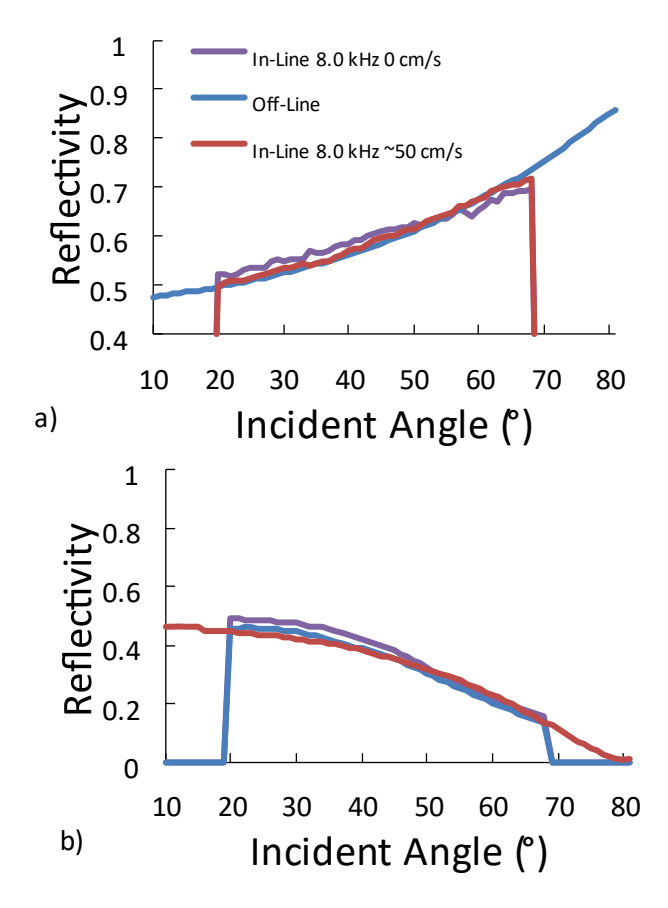


Fig. 8: a) TE and b) TM reflectivity curves vs. incident angle for In-line scatterometer 8.0 kHz at: 0 cm/s and 50 cm/s. and off-line for the native oxide layer.

Table 1: Comparison table of all system fitted results and RMSE for TE Polarization on the native oxide layer.

System	RMSE TE	Web Speed (cm/s)	SiO <sub>2</sub> Fitted Values TE (nm)	
Ellipsometry	5.34×10 <sup>-3</sup>	0	1.36	
Off-line Scatterometer	8.04×10 <sup>-3</sup>	0	1.9	
8.0 kHz In-line Scatterometer	1.29×10 <sup>-2</sup>	0	1.35	

8.0 kHz In-line Scatterometer	2.41×10 <sup>-2</sup>	~2.6 cm/s	1.38
8.0 kHz In-line Scatterometer	9.27×10 <sup>-3</sup>	~50.0 cm/s	1.36

Table 2: Comparison table of all system fitted results and RMSE for TM Polarization on the native oxide layer.

System	RMSE TE	Web Speed (cm/s)	SiO <sub>2</sub> Fitted Values TE (nm)	
Ellipsometry	5.34×10 <sup>-3</sup>	0	1.36	
Off-line Scatterometer	6.58×10 <sup>-3</sup>	0	2.2	
2.5 kHz In-line Scatterometer	1.18×10 <sup>-3</sup>	0	1.30	
8.0 kHz In-line Scatterometer	1.27×10 <sup>-2</sup>	0	1.31	
8.0 kHz In-line Scatterometer	1.58×10 <sup>-2</sup>	~2.6 cm/s	1.36	
8.0 kHz In-line Scatterometer	1.44×10 <sup>-2</sup>	~50.0 cm/s	1.36	

#### 5.2 Silicon Wafer with ~100-nm SiO<sub>2</sub> Over layer

Similarly, the thicker oxide layer on the silicon wafer was measured by using ellipsometry and compared with off-line, and in-line scatterometers. Fig. 9 present the TE and the TM reflection curve of 8.0 kHz in-line scatterometer (at 0 cm/second and 50 cm/second) vs. off-line on the thin ( $\sim$ 100 nm) SiO<sub>2</sub> layer. Tables 3 and 4 present the RMSE from each system and the oxide fitted values on the thin ( $\sim$ 100 nm) SiO<sub>2</sub> layer.

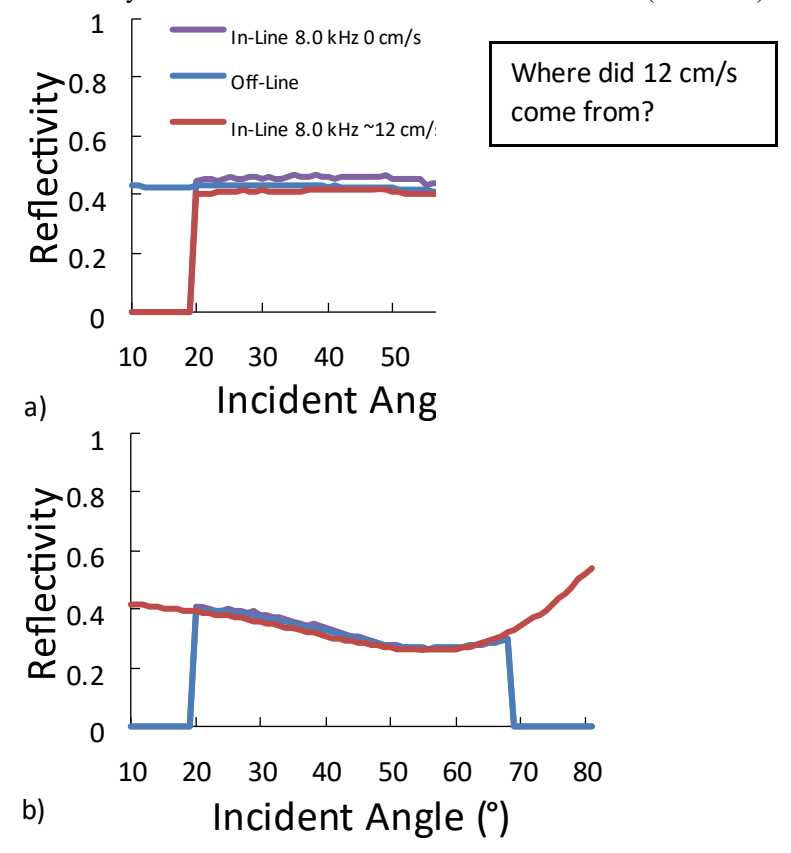


Fig. 9: a) TE and b) TM reflectivity curves vs. incident angle for In-line scatterometer  $8.0 \, \text{kHz}$  at:  $0 \, \text{cm/s}$  and  $0.6 \, \text{cm/s}$ . and simulation on the thin ( $\sim 100 \, \text{nm}$ ) SiO2 layer.

Table 3: Comparison table of all system fitted results and RMSE for TE Polarization on the thin (~100 nm) SiO2 layer.

System	RMSE TE	Web Speed (cm/s)	SiO <sub>2</sub> Fitted Values TE (nm)	
Ellipsometry	1.45×10 <sup>-3</sup>	0	114.0	
Off-line Scatterometer	3.91×10 <sup>-3</sup>	0	114.0	
2.5 kHz In-line Scatterometer	3.13×10 <sup>-3</sup>	0	114.4	
8.0 kHz In-line Scatterometer	8.14×10 <sup>-2</sup>	0	114.8	
8.0 kHz In-line Scatterometer	4.99×10 <sup>-2</sup>	~2.6 cm/s	115.2	
8.0 kHz In-line Scatterometer	9.50×10 <sup>-2</sup>	~50.0 cm/s	113.3	

Table 4: Comparison table of all system fitted results and RMSE for TM Polarization on the thin (~100 nm) SiO2 layer.

System	RMSE TE	Web Speed (cm/s)	SiO <sub>2</sub> Fitted Values TE (nm)	
Ellipsometry	1.45×10 <sup>-3</sup>	0	114.0	
Off-line Scatterometer	6.69×10 <sup>-3</sup>	0	114.0	
2.5 kHz In-line Scatterometer	3.90×10 <sup>-3</sup>	0	113.9	
8.0 kHz In-line Scatterometer	6.61×10 <sup>-2</sup>	0	114.2	
8.0 kHz In-line Scatterometer	9.06×10 <sup>-2</sup>	~2.6 cm/s	112.5	
8.0 kHz In-line Scatterometer	9.94×10 <sup>-2</sup>	~50.0 cm/s	113.5	

#### 5.3 1D Undercut Nanoscale Al Lines on Silicon Wafer

For the 1D patterned structures, the sample was measured using and both the off-line and in-line 8.0 kHz scatterometers. The polarization was perpendicular to the orientation of the lines (low reflectivity, high transmission). The high reflectivity polarization conditions do not offer a sufficient dynamic range for metrology purposes  $^{13}$ . All results were fitted to a simulation and 5 parameters were extracted from the fit to RCWA code simulation, including: period (P), antireflective coat height (IH), antireflective coat width (IW), aluminum height (AIH), aluminum width (AIW). Fig. 10 presents the TE and the TM reflection curve of 8.0 kHz in-line scatterometer (at 0 and  $\sim$ 50 cm/second) vs. the simulation on the 1D undercut Al lines. Tables 5 present in-line scatterometry fitted results on the 1D undercut Al lines. Web speed (WS) is also shown on table 5. Clearly, SEM is a tool that does not provide precise measurements. The SEM values are an approximation value of the actual physical structure size. Our fitted results gave us a more accurate value of the pattern structures. Only 5 parameters were fitted on this simulation.

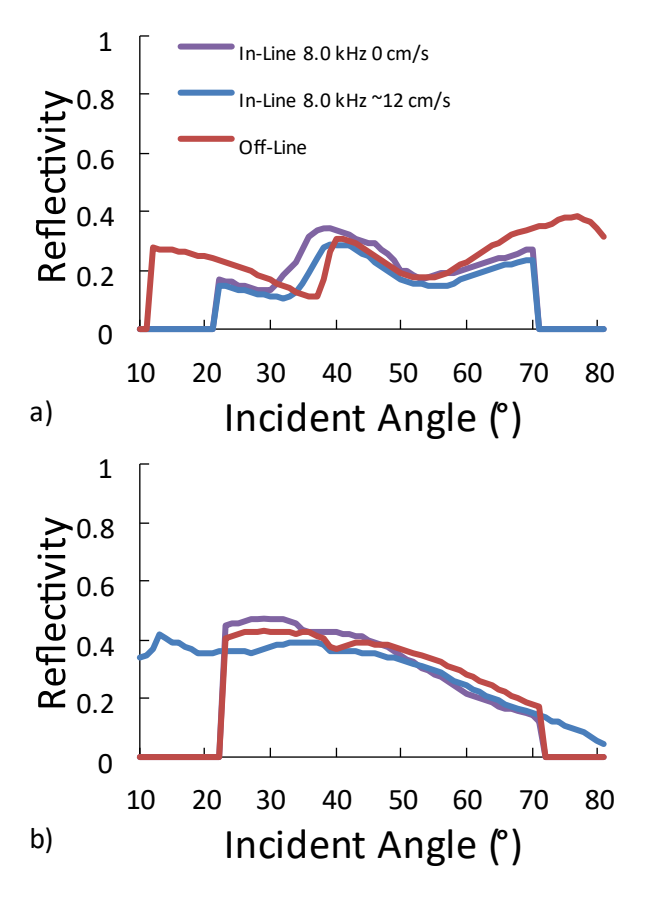


Fig. 10: a) TE and b) TM Reflectivity curve vs. incident angle for 1D undercut Al lines. Table

5: In-line scatterometry fitted results on the 1D undercut Al lines compared with SEM.

System	WS (cm/s)	RMSE	P (nm)	IH (nm)	IW (nm)	AlH (nm)	AlW (nm)
8.0 kHz In-line Scatterometer	0	8.54×10 <sup>-2</sup>	491.2	144.7	151.8	90.8	334.1
8.0 kHz In-line Scatterometer	~50.0 above	6.70×10 <sup>-2</sup>	485.0	158.1	158.0	102.8	324.6
SEM	0		~503	~149	~140	~91	~341

#### 5.4 2D Silicon Nanotubes on Silicon Wafer

Finally, for the 2D patterned structures, the sample was measured using the in-line  $8.0\,\mathrm{kHz}$  scatterometer. All results were compared to off-line and  $2.5\,\mathrm{kHz}$  in-line scatterometers. For this structure, we did not fit to a simulation, however experimental results reflection as function of angle has similar pattern. FDTD simulation will be needed due to the complex structure shown on the 2D nanotubes structures. Fig. 11 present the TE and the TM reflection curve of  $8.0\,\mathrm{kHz}$  in-line scatterometer (at 0 and  $\sim 50\,\mathrm{cm/second}$ ) vs. off-line on the 2D silicon nanotubes. Clearly our system can scan and characterize complex structures at high-speed web movement during R2R fabrication processes. A well-defined library with a detailed structure simulation will ensure even a better fitting process. This translates to better metrology processes during real-time fabrication under moving conditions.

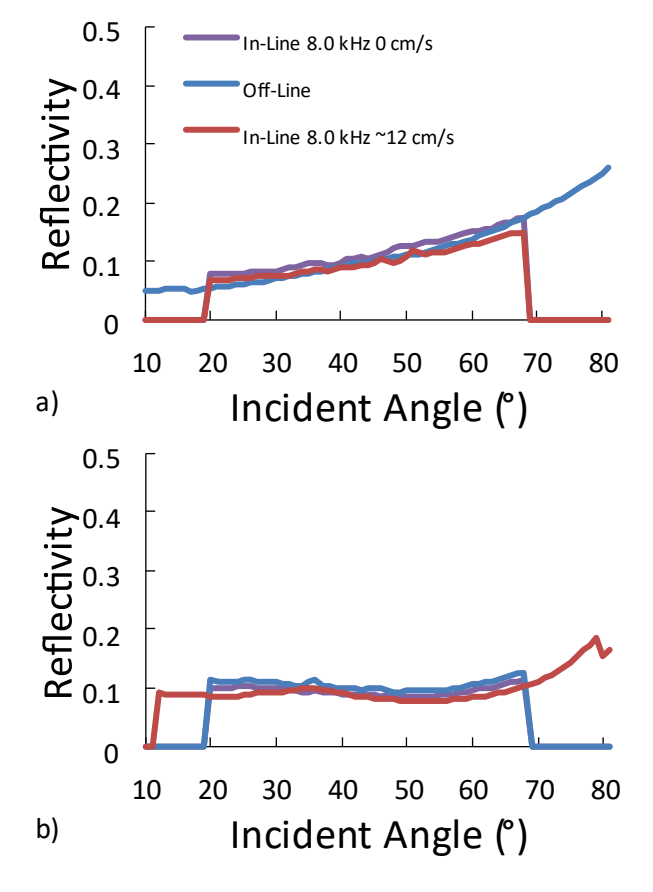


Fig. 11: a) TE and b) TM reflectivity versus incident angle for 2D nano-tubes.

#### 6. CONCLUSIONS/FUTURE WORK

This work demonstrates an in-line scatterometer system that can be implemented for real-time R2R and printed electronics fabrication processes. The 8.0 kHz scatterometer allows characterization under nondestructive, noncontact, and high-speed conditions. Angular optical scatterometry is the only nanoscale dimensional metrology approach that can be adapted to real-time nanomanufacturing processes. The 8.0 kHz resonant scanner scans a full cycle trace and retrace in 125 µs. The system has proven scanning capabilities and can be implemented without interfering a real time web process. The highspeed measurements are in excellent agreement with other approaches (ellipsometry) and off-line (static) scatterometry measurements. The system has shown potential for detecting printing defects including non-filing and pin holes. More experimental work will be performed to determine the ultimate resolution limits of the defect detection during real-time fabrication processes. The angular range can be increased by changing the optical characteristics of the parabolic mirror (size and focal length). In-line optical angular scatterometry is a powerful tool that has many applications in the manufacturing and semiconductor industry.

### References

- [1] 2020 International Roadmap for Devices and Systems (https:/irds.ieee.org).
- [2] N.G. Orji, M. Badaroglu, B.M. Barnes, C. Beitia, B.D. Bunday, U. Celano, R.J. Kline, MM. Neisser, Y. Obeng and A.E.Vladar, "Metrology for the next generation of semiconductor devices," Nature Electron. (1), 532-547 (2018).
- [3] J.A. Liddle, G.M. Gallatin. "Lithography, Metrology, and Nanomanufacturing." Nanoscale (3), 2679-2688 (2011).
- [4] M.A.M. Leenen, V. Arning, H. Thiem, J. Steiger and R. Anselmann, "Printable electronics: flexibility for the future," Phys. Stat. Sol. A206, 588-597 (2009).
- [5] S. V. Sreenivasan. "Nanoscale Manufacturing enabled by Imprint Lithography." MRS Bull (33), 854 (2008).

- [6] J.J. Wang, F. Walters, X. Liu, P. Sciortino and X. Deng. "High-Performance, Large Area, Deep Ultraviolet to Infrared Polarizers Based on 40 nm line/ 78 nm Space Nanowire Grid." Appl. Phys. Lett. (90), 061104 (2007).
- [7] D. Dixit, A. Green, E.R. Hosier, V. Kamineni, M.E. Prell, N. Keller, J. Race, J.S. Chun, M. O'Sullivan, P. Khare, W. Montgomery and A.C. Diebold. "Optical Critical Dimension Metrology for Directed Self-Assembly Assisted Contact Hole Shrink." J. Micro/Nanolith. MEMS MOEMS 15 (1), 014004 (2016).
- [8] V. F. Paz, S. Paterhansel, K. Frenner, and W. Osten. "Solving the inverse grating problem by white light interference Fourier scatterometry." Nat Sci. & Appl. (1) e36 (2012).
- [9] R. Zhu, S.R.J. Brueck, N. Dawson, T. Busani, P. Joseph, S. Singhal and S.V. Sreenivasan. "Scatterometry for Nanoimprint Lithography." J. Vac. Sci. and Technol. (B34), 06K503-1-10 (2016).
- [10] B. Gawlik, C. Barrera, E. T. Yu, and S.V. Sreenivasan. "Hyperspectral imaging for high-throughtput, spatially resolved spectroscopic scatterometry of silicon nanopillars arrays." Opt. Exp. (28), 10 14209-14221 (2020).
- [11] B. J. Rice, H. Cao, M. Grumski and J. Roberts. "The Limits of CD Metrology." Microelec. Engr. (83) 1023-1029 (2006).
- [12] N.G. Orji, M. Badaroglu, B.M. Barnes, C. Beitia, B.D. Bunday, U. Celano, R.J. Kline, M. Neisser, Y. Obeng and A.E. Vladar. "Metrology for the next generation of semiconductor devices." Nat Elec (1), 532-547 (2018).
- [13] R. Zhu, J.J. Faria-Briceno, S.R.J. Brueck, P. Joseph, S. Singhal and S.V. Sreenivasan. "Nanoscale Limits of Angular Optical Scatterometry." AIP Adv. (10), 015140 (2020).
- [14] D. Dixit, N. Keller, T. Kagalwala, F. Recchia, Y. Lifshitz, A. Elia, V. Todi, J. Fronheiser A. Valid. "Advanced Applications of Scatterometry Based Optical Metrology." Proc. SPIE 10145, 101451H (2017).
- [15] J.J. Faria-Briceno, R. Zhu, V. Sasidharan, A. Neumann, S. Singhal, S.V. Sreenivasan and S.R.J. Brueck. "Optical Angular Scatterometry: In-line metrology Approach for Roll-to-Rolland Nano-Imprint Fabrication." J. Vac. Sci. Technol. (37), 052904 (2019).
- [16] G.L. Whitworth, A. Francone, C.M. Sotomayor-Torres, and N. Kehagias. "Real-time Optical Dimension Metrology via Diffractometry for Nanofabrication." Sci. Rep. (10), 5371 (2020).
- [17] C.M. Herzinger, B. Johs, W.A. McGahan, W. Paulson. "A Multi-sample, multi-wavelength, multi-angle investigation of the interface layer between silicon and thermally grown silicon dioxide" Thin Solid Films (313), 281-285 (1998).
- [18] J.J. Faria-Briceno, A. Neumann, A., P.R. Schunk, S.R.J. Brueck. "Measuring Liquid Drop Properties on Nanoscale 1D Patterned Photoresist Structures." Sci. Rep. (9), 5723 (2019).

#### ACKNOWLEDGMENT

This work is based upon work supported primarily by the National Science Foundation under Cooperative Agreement No. EEC-1160494. Any opinions, findings and conclusions or recommendations expressed in this material are those of the author(s) and do not necessarily reflect the views of the National Science Foundation.

#### **COMPETING INTERESTS**

The authors declare no competing interests.